International Tables for Crystallography (2006). Vol. D, Chapter 1.4, pp. 99–104.

1.4. Thermal expansion

By H. Küppers

1.4.1. Definition, symmetry and representation surfaces

If the temperature T of a solid is raised by an amount ΔT, a deformation takes place that is described by the strain tensor u_{ij}:

$$u_{ij} = \alpha_{ij}\Delta T. \qquad (1.4.1.1)$$

The quantities α_{ij} are the coefficients of thermal expansion. They have dimensions of T^{-1} and are usually given in units of 10^{-6} K^{-1}. Since u_{ij} is a symmetrical polar tensor of second rank and T is a scalar, α_{ij} is a symmetrical polar tensor of second rank ($\alpha_{ij} = \alpha_{ji}$). According to the properties of the strain tensor u_{ij} (*cf.* Section 1.3.1.3.2), the 'volume thermal expansion', β, is given by the (invariant) trace of the 'linear' coefficients α_{ij}.

$$\beta = \frac{1}{V}\frac{\Delta V}{\Delta T} = \alpha_{11} + \alpha_{22} + \alpha_{33} = \text{trace } (\alpha_{ij}). \qquad (1.4.1.2)$$

The magnitudes of thermal expansion in different directions, α'_{11}, can be visualized in the following ways:

(1) The representation quadric (*cf.* Section 1.1.3.5.2)

$$\alpha_{ij}x_ix_j = C \qquad (1.4.1.3)$$

can be transformed to principal axes X_1, X_2 and X_3 with principal values α_1, α_2 and α_3:

$$\alpha_1X_1^2 + \alpha_2X_2^2 + \alpha_3X_3^2 = C.$$

The length of any radius vector leading to the surface of the quadric ($C = 1$) represents the reciprocal of the square root of thermal expansion along that direction, $\alpha'_{11} = a_{1i}a_{1j}\alpha_{ij}$ (a_{kl} are the direction cosines of the particular direction).

If all α_i are positive, the quadric ($C = +1$) is represented by an ellipsoid, whose semiaxes have lengths $1/\sqrt{\alpha_i}$. In this case, the square of the reciprocal length of radius vector $\mathbf{r}$, r^{-2}, represents the amount of positive expansion in the particular direction, *i.e.* a *dilation* with increasing temperature. If all α_i are negative, C is set to -1. Then, the quadric is again an ellipsoid, and r^{-2} represents a negative expansion, *i.e.* a *contraction* with increasing temperature.

If the α_i have different signs, the quadric is a hyperboloid. The asymptotic cone represents directions along which no thermal expansion occurs ($\alpha'_{11} = 0$).

If one of the α_i is negative, let us first choose $C = +1$. Then, the hyperboloid has one (belt-like) sheet (*cf.* Fig. 1.3.1.3) and the squares of reciprocal lengths of radius vectors leading to points on this sheet represent positive expansions (dilatations) along the particular directions. Along directions where the hyperboloid has no real values, negative expansions occur. To visualize these, C is set to -1. The resulting hyperboloid has two (cap-like) sheets (*cf.* Fig. 1.3.1.3) and r^{-2} represents the amount of contraction along the particular direction.

If two of the α_i are negative, the situation is complementary to the previous case.

(2) A crystal sample having spherical shape (radius = 1 at temperature T) will change shape, after a temperature increase ΔT, to an ellipsoid with principal axes $(1 + \alpha_1\Delta T)$, $(1 + \alpha_2\Delta T)$ and $(1 + \alpha_3\Delta T)$. This 'strain ellipsoid' is represented by the formula

$$\frac{X_1^2}{(1+\alpha_1\Delta T)^2} + \frac{X_2^2}{(1+\alpha_2\Delta T)^2} + \frac{X_3^2}{(1+\alpha_3\Delta T)^2} = 1.$$

Whereas the strain quadric (1.4.1.3) may be a real or imaginary ellipsoid or a hyperboloid, the strain ellipsoid is always a real ellipsoid.

(3) The magnitude of thermal expansion in a certain direction (the longitudinal effect), α'_{11}, if plotted as radius vector, yields an oval:

$$(\alpha_1X_1^2 + \alpha_2X_2^2 + \alpha_3X_3^2)^2 = (X_1^2 + X_2^2 + X_3^2)^3.$$

If spherical coordinates (φ, ϑ) are used to specify the direction, the length of $\mathbf{r}$ is

$$|\mathbf{r}| = \alpha'_{11} = (\alpha_1\cos^2\varphi + \alpha_2\sin^2\varphi)\sin^2\vartheta + \alpha_3\cos^2\vartheta. \qquad (1.4.1.4)$$

Sections through this representation surface are called polar diagrams.

The three possible graphical representations are shown in Fig. 1.4.1.1.

The maximum number of independent components of the tensor α_{ij} is six (in the triclinic system). With increasing symmetry, this number decreases as described in Chapter 1.1. Accordingly, the directions and lengths of the principal axes of the representation surfaces are restricted as described in Chapter 1.3 (*e.g.* in hexagonal, trigonal and tetragonal crystals, the representation surfaces are rotational sheets and the rotation axis is parallel to the n-fold axis). The essential results of these symmetry considerations, as deduced in Chapter 1.1 and relevant for thermal expansion, are compiled in Table 1.4.1.1.

The coefficients of thermal expansion depend on temperature. Therefore, the directions of the principal axes of the quadrics in triclinic and monoclinic crystals change with temperature (except the principal axis parallel to the twofold axis in monoclinic crystals).

The thermal expansion of a polycrystalline material can be approximately calculated if the α_{ij} tensor of the single crystal is known. Assuming that the grains are small and of comparable size, and that the orientations of the crystallites are randomly distributed, the following average of α'_{11} [(1.4.1.4)] can be calculated:

$$\bar{\alpha} = \frac{1}{4\pi}\int_0^{2\pi}\int_0^{\pi}\alpha'_{11}\sin\vartheta\,\mathrm{d}\vartheta\,\mathrm{d}\varphi = \tfrac{1}{3}(\alpha_1 + \alpha_2 + \alpha_3).$$

If the polycrystal consists of different phases, a similar procedure can be performed if the contribution of each phase is considered with an appropriate weight.

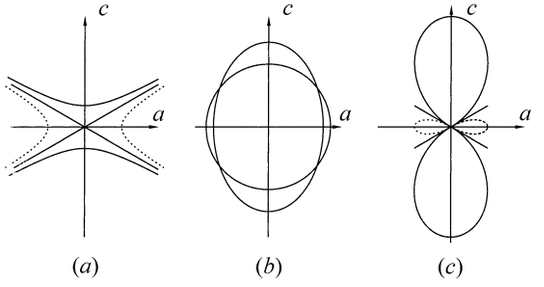

Fig. 1.4.1.1. Sections (ac plane) of representation surfaces for a trigonal (or tetragonal or hexagonal) crystal with $\alpha_{11} = \alpha_{22} = -1$ and $\alpha_{33} = +3 \times 10^{-5}$ K^{-1} (similar to calcite). (a) Quadric, (b) strain ellipsoid (greatly exaggerated), (c) polar diagram. The c axis is the axis of revolution. Sectors with negative expansions are dashed.

It should be mentioned that the true situation is more complicated. The grain boundaries of anisotropic polycrystalline solids are subject to considerable stresses because the neighbouring grains have different amounts of expansion or contraction. These stresses may cause local plastic deformation and cracks may open up between or within the grains. These phenomena can lead to a hysteresis behaviour when the sample is heated up or cooled down. Of course, in polycrystals of a cubic crystal species, these problems do not occur.

If the polycrystalline sample exhibits a texture, the orientation distribution function (ODF) has to be considered in the averaging process. The resulting overall symmetry of a textured polycrystal is usually $\frac{\infty}{m}m$ (see Section 1.1.4.7.4.2), showing the same tensor form as hexagonal crystals (Table 1.4.1.1), or *mmm*.

Table 1.4.1.1. *Shape of the quadric and symmetry restrictions*

System	Quadric: Shape	Quadric: Direction of principal axes	No. of independent components	Nonzero components
Triclinic	General ellipsoid or hyperboloid	No restrictions	6	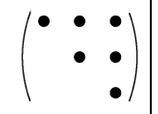
Monoclinic		One axis parallel to twofold axis (**b**)	4	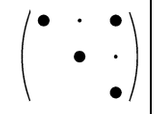
Orthorhombic		Parallel to crystallographic axes	3	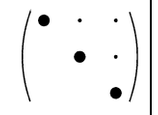
Trigonal, tetragonal, hexagonal	Revolution ellipsoid or hyperboloid	*c* axis is revolution axis	2	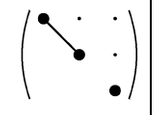
Cubic, isotropic media	Sphere	Arbitrary, not defined	1	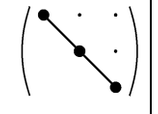

1.4.2. Grüneisen relation

Thermal expansion of a solid is a consequence of the anharmonicity of interatomic forces (see also Section 2.1.2.8). If the potentials were harmonic, the atoms would oscillate (even with large amplitudes) symmetrically about their equilibrium positions and their mean central position would remain unchanged. In order to describe thermal expansion, the anharmonicity is most conveniently accounted for by means of the so-called 'quasiharmonic approximation', assuming the lattice vibration frequencies ω to be independent of temperature but dependent on volume $[(\partial\omega/\partial V) \neq 0]$. Anharmonicity is taken into account by letting the crystal expand, but it is assumed that the atoms vibrate about their new equilibrium positions harmonically, *i.e.* lattice dynamics are still treated in the harmonic approximation. The assumption $(\partial\omega/\partial V) = 0$, which is made for the harmonic oscillator, is a generalization of the postulate that the frequency of a harmonic oscillator does not depend on the amplitude of vibration.

This approach leads, as demonstrated below, to the Grüneisen relation, which combines thermal expansion with other material constants and, additionally, gives an approximate description of the temperature dependence of thermal expansion (*cf.* Krishnan *et al.*, 1979; Barron, 1998).

For isotropic media, the volume expansion β $[= 3\alpha = \alpha_{11} + \alpha_{22} + \alpha_{33}]$, *cf.* (1.4.1.2), can be expressed by the thermodynamic relation

$$\beta = \frac{1}{V}\left(\frac{\partial V}{\partial T}\right)_p = -\frac{1}{V}\left(\frac{\partial V}{\partial p}\right)_T\left(\frac{\partial p}{\partial T}\right)_V = \kappa\left(\frac{\partial p}{\partial T}\right)_V, \qquad (1.4.2.1)$$

κ being the isothermal compressibility. To obtain the quantity $(\partial p/\partial T)_V$, the pressure p is deduced from the free energy F, whose differential is $\mathrm{d}F = -S\,\mathrm{d}T - p\,\mathrm{d}V$, *i.e.* from

$$p = -(\partial F/\partial V)_T. \qquad (1.4.2.2)$$

In a crystal consisting of N unit cells with p atoms in each unit cell, there are $3p$ normal modes with frequencies ω_s (denoted by an index s running from 1 to $3p$) and with N allowed wavevectors $\mathbf{q}_t$ (denoted by an index t running from 1 to N). Each normal mode $\omega_s(\mathbf{q}_t)$ contributes to the free energy by the amount

$$f_{s,t} = \frac{\hbar}{2}\omega_s(\mathbf{q}_t) + kT\ln\left[1 - \exp\left(-\frac{\hbar\omega_s(\mathbf{q}_t)}{kT}\right)\right]. \qquad (1.4.2.3)$$

The total free energy amounts, therefore, to

$$F = \sum_{s=1}^{3p}\sum_{t=1}^{N} f_{s,t}$$

$$= \sum_{s=1}^{3p}\sum_{t=1}^{N}\left\{\frac{\hbar}{2}\omega_s(\mathbf{q}_t) + kT\ln\left[1 - \exp\left(-\frac{\hbar\omega_s(\mathbf{q}_t)}{kT}\right)\right]\right\}. \qquad (1.4.2.4)$$

From (1.4.2.2)

$$p = -\left(\frac{\partial F}{\partial V}\right)_T$$

$$= -\sum_{s=1}^{3p}\sum_{t=1}^{N}\left\{\frac{\hbar}{2}\frac{\partial\omega_s}{\partial V} + \frac{\exp(-\hbar\omega_s/kT)\hbar(\partial\omega_s/\partial V)}{1 - \exp(-\hbar\omega_s/kT)}\right\}. \qquad (1.4.2.5)$$

The last term can be written as

$$\frac{\hbar(\partial\omega_s/\partial V)}{\exp(\hbar\omega_s/kT) - 1} = \hbar n(\omega_s(\mathbf{q}_t), T)\frac{\partial\omega_s}{\partial V}, \qquad (1.4.2.6)$$

where $n(\omega_s, T)$ is the Bose–Einstein distribution

$$n(\omega_s, T) = \frac{1}{\exp(\hbar\omega_s/kT) - 1}. \quad (1.4.2.7)$$

Differentiation of (1.4.2.5) and (1.4.2.6) with respect to temperature at constant volume [see (1.4.2.1)] yields

$$\left(\frac{\partial p}{\partial T}\right)_V = -\sum_s \sum_t \hbar \frac{\partial n(\omega_s, T)}{\partial T} \frac{\partial \omega_s(\mathbf{q}_t)}{\partial V} = -\sum_s \sum_t c_{s,t}^V \frac{1}{\omega_s(\mathbf{q}_t)} \frac{\partial \omega_s(\mathbf{q}_t)}{\partial V} \quad (1.4.2.8)$$

with

$$c_{s,t}^V = \hbar\omega_s(\mathbf{q}_t) \frac{\partial n(\omega_s, T)}{\partial T} = k \frac{(\hbar\omega_s/kT)^2 \exp(\hbar\omega_s/kT)}{[\exp(\hbar\omega_s/kT) - 1]^2}. \quad (1.4.2.9)$$

This quantity, $c_{s,t}^V$ (the Einstein function), is the well known contribution of the normal mode $\omega_s(\mathbf{q}_t)$ to the specific heat (at constant volume):

$$c^V = \sum_s \sum_t c_{s,t}^V = \sum_s \sum_t \hbar\omega_s(\mathbf{q}_t) \frac{\partial n(\omega_s, T)}{\partial T}. \quad (1.4.2.10)$$

Equation (1.4.2.8) can be simplified by the introduction of an 'individual Grüneisen parameter' $\gamma_{s,t}$ for each normal mode $\omega_s(\mathbf{q}_t)$:

$$\gamma_{s,t} = -\frac{V}{\omega_s(\mathbf{q})_t} \frac{\partial \omega_s(\mathbf{q})_t}{\partial V} = -\frac{\partial[\ln \omega_s(\mathbf{q}_t)]}{\partial(\ln V)}. \quad (1.4.2.11)$$

Equation (1.4.2.8) then reads [with (1.4.2.1)]

$$\left(\frac{\partial p}{\partial T}\right)_V = \frac{1}{V} \sum_s \sum_t c_{s,t}^V \gamma_{s,t} = \frac{\beta}{\kappa}. \quad (1.4.2.12)$$

Based on these individual parameters $\gamma_{s,t}$, an average (or overall mode-independent) Grüneisen parameter $\bar{\gamma}$ can be defined as

$$\bar{\gamma} = \frac{\sum\sum \gamma_{s,t} c_{s,t}^V}{\sum\sum c_{s,t}^V} = \frac{\sum\sum \gamma_{s,t} c_{s,t}^V}{c^V}. \quad (1.4.2.13)$$

In this averaging process, the contribution of each normal mode to $\bar{\gamma}$ is weighted in the same way as it contributes to the specific heat c^V [see (1.4.2.10)]. Equations (1.4.2.12) and (1.4.2.13) lead to the Grüneisen relation

$$\beta = \bar{\gamma} \frac{\kappa c^V}{V}. \quad (1.4.2.14)$$

The above derivation was made for isotropic media. For anisotropic media, $\Delta V/V$ is replaced by the strain u_{kl} and κ^{-1} is replaced by the stiffness tensor c_{ijkl} [*cf.* Chapter 2.1 and equation (2.1.2.75)]. Then the Grüneisen parameter turns out to be a second-rank tensor γ_{ij}:

$$\gamma_{ij} = \frac{V}{c^V} c_{ijkl}^T \alpha_{kl}. \quad (1.4.2.15)$$

In the Debye approximation, the mode frequencies scale linearly with the cut-off frequency ω_D. Therefore, with $\hbar\omega_D = kT_D$, the average isotropic Grüneisen parameter is calculated to be

$$\gamma_D = -\frac{V}{\omega_D} \frac{\partial \omega_D}{\partial V} = -\frac{V}{T_D} \frac{\partial T_D}{\partial V} = -\frac{\partial(\ln T_D)}{\partial(\ln V)}.$$

Since, in the Debye theory, T_D is independent of temperature, γ_D turns out to be independent of temperature. As κ and V are only weakly temperature dependent, the thermal expansion β should then, according to (1.4.2.14), roughly behave like c^V, *i.e.* β should be proportional to T^3 at very low temperatures, and should be approximately constant for $T \gg T_D$ (the Dulong–Petit law). This behaviour is found to be approximately satisfied for many compounds, even with different types of interatomic interaction, and γ takes values roughly between 1 and 2. Even in the case of crystals with highly anisotropic elastic and thermal behaviour, the three principal values of the tensor γ_{ij} [(1.4.2.15)] are comparably uniform, having values of about 2 (Küppers, 1974).

Effectively, γ shows a certain more or less pronounced dependence on temperature. The individual $\gamma_{s,t}$ are assumed to be temperature independent. However, being an average over the whole spectrum of excited modes [*cf.* (1.4.2.13)], $\bar{\gamma}$ will not necessarily have the same value at low temperatures (when only low frequencies are excited) as at high temperatures (when all modes are excited). Two limiting cases can be considered:

(1) At very high temperatures, all normal modes contribute by an equal amount and the overall $\bar{\gamma}$ becomes simply the mean value of all $\gamma_{s,t}$.

$$\gamma_\infty = \frac{1}{3pN} \sum_s^{3p} \sum_t^N \gamma_{s,t}.$$

(2) At very low temperatures, only the lower frequencies contribute. If only the acoustic branches are considered, $\bar{\gamma}$ can be related to the velocities of elastic waves. In the long-wavelength limit, dispersion is neglected, *i.e.* $|\mathbf{q}|$ is proportional to ω:

$$|\mathbf{q}_t| = \frac{\omega_s(\mathbf{q}_t)}{v_s(\varphi, \vartheta)}, \quad (1.4.2.16)$$

where $v_s(\varphi, \vartheta)$ $(s = 1, 2, 3)$ describes the velocities of the three elastic waves propagating in a direction (φ, ϑ). The density of vibrational states for each acoustic branch in reciprocal space increases with $q^2\,\mathrm{d}q$. From (1.4.2.16), it follows that the number of normal modes in an increment of solid angle in $\mathbf{q}$ space, $\mathrm{d}\Omega = \sin\vartheta\,\mathrm{d}\vartheta\,\mathrm{d}\varphi$, within a frequency interval ω to $\omega + \mathrm{d}\omega$, is proportional to $(\omega^2\,\mathrm{d}\omega\,\mathrm{d}\Omega)/v^3$. The summation over t can be converted into an integration over ω and Ω, leading to

$$\gamma_0 = \frac{\sum_{s=1}^3 \int \frac{\gamma_s(\vartheta, \varphi)\,\mathrm{d}\Omega}{v_s^3(\vartheta, \varphi)}}{\sum_{s=1}^3 \int \frac{\mathrm{d}\Omega}{v^3(\vartheta, \varphi)}}.$$

The $v_s(\varphi, \vartheta)$ can be calculated if the elastic constants are known. For isotropic solids, the term $\sum v_s^{-3}$ can be replaced (as done in Debye's theory of heat capacity) by $(v_l^{-3} + 2v_{\mathrm{tr}}^{-3})$, with v_l being the velocity of the longitudinal wave and v_{tr} the velocity of the transverse waves.

In metals, the conduction electrons and magnetic interactions yield contributions to the free energy and to the specific heat. Accordingly, expression (1.4.2.14) can be augmented by introduction of an 'electronic Grüneisen parameter', γ_e, and a 'magnetic Grüneisen parameter', γ_m, in addition to the 'lattice Grüneisen parameter', γ_l, considered so far:

$$\beta = \frac{\kappa}{V}(\gamma_l c_l^V + \gamma_e c_e^V + \gamma_m c_m^V).$$

1.4.3. Experimental methods

1.4.3.1. *General remarks*

Although the strain tensor u_{ij} and the thermal expansion tensor α_{ij} in general contain components with $i \neq j$ (shear strains), in practice only longitudinal effects, *i.e.* relative length changes $\Delta l/l$ with temperature changes ΔT, are measured along different directions and the results are later transformed to a common coordinate system. Diffraction methods directly yield this ratio $\Delta l/l$. Other measuring techniques require separate measurements of Δl and l. The error in the measurement of l can

usually be neglected. Thus, the accuracies of Δl and ΔT limit the accuracy of thermal expansion coefficients. The temperature interval ΔT is determined by two measurements of temperatures $T_2 > T_1$, with $T_2 - T_1 = \Delta T$. To increase the accuracy of the difference ΔT, this interval should be large. The measured thermal expansion $\Delta l/(l\Delta T)$ is usually assigned to a temperature at the midpoint of the temperature interval, $T_0 = (T_2 - T_1)/2$. This procedure is only justified if thermal expansion does not depend on temperature.

Since, in fact, thermal expansion depends on temperature, in principle, smaller intervals should be chosen, which, in turn, enlarge the error of ΔT. Here, a compromise has to be made. Sometimes, after completion of a first run and after reviewing the preliminary course of $\alpha(T)$, it is necessary to repeat some measurements using smaller temperature intervals in temperature ranges with large curvatures.

The more-or-less curved course of $\alpha_{ij}(T)$ is usually fitted by polynomials in powers of temperature. Here, those T terms should be selected that are physically meaningful in the particular temperature range. For the low-temperature behaviour of a metal, a polynomial of type $\alpha = AT + BT^3 + CT^5$ should be chosen. For minerals at higher temperatures, a polynomial $\alpha = \alpha_0 + AT + BT^{-1} + CT^{-2}$ is used (Saxena & Shen, 1992).

Temperature is usually measured by thermocouples and, in the cases of optical or electrical measurements (Sections 1.4.3.3 and 1.4.3.4) and at low temperatures also by platinum resistance thermometers. Above 1100 K, optical pyrometers can be used.

In order to measure the thermal expansion of a crystal, at least as many independent measurements are necessary as the tensor has independent components (fourth column in Table 1.4.1.1). It is advisable, however, to carry out more measurements than are necessary. In this case (of redundancy), a 'best' set of tensor components is to be determined by least-squares methods as described below.

Let us assume the most general case of a triclinic crystal, where $m > 6$ independent measurements of thermal expansions b_k $(k = 1, \ldots, m)$ were performed along m different directions with direction cosines $(\alpha_{1j})_k$ $(j = 1, 2, 3)$ with respect to the chosen coordinate system. Each measurement b_k is related to the six unknown tensor components α_{ij} (to be determined) by

$$b_k = (\alpha'_{11})_k = (\alpha_{1i})_k(\alpha_{1j})_k\alpha_{ij}. \qquad (1.4.3.1)$$

If the α_{ij} are replaced by α_γ $(\gamma = 1, \ldots, 6)$, using Voigt's one-index notation (Section 1.1.4.10.2), then $b_k = C_{k\gamma}\alpha_\gamma$ represents an overdetermined inhomogeneous system of m linear equations for the six unknowns α_γ. The coefficients $C_{k\gamma}$, forming an $m \times 6$ matrix, are products containing direction cosines according to (1.4.3.1). The solution is obtained after several matrix calculations which are indicated by the formula (Nye, 1985)

$$\alpha_\gamma = \left\{\left[(C^t_{l\delta} \cdot C_{l\varepsilon})^{-1}\right]_{\gamma\eta} C^t_{k\eta}\right\} b_k$$
$$(\gamma, \delta, \varepsilon, \eta = 1, \ldots, 6; \quad l, k = 1, \ldots, m),$$

where a superscript 't' means transposed.

Instead of determining the tensor components of a triclinic or monoclinic crystal in a direct way, as outlined above, it is also possible to determine first the temperature change of the crystallographic unit cell and then, by formulae given *e.g.* by Schlenker *et al.* (1978), to deduce the tensor components α_{ij}. The direct approach is recommended, however, for reasons of the propagation of errors (Jessen & Küppers, 1991).

The experimental techniques of measuring relative length changes $\Delta l/l$ that are most widely used include diffraction, optical interferometry, pushrod dilatometry and electrical capacitance methods. If the specimens available are very small and/or irregular in shape, only diffraction methods can be used. The other methods require single-crystal parallelepipedal samples with at least 5 mm side lengths.

1.4.3.2. *Diffraction*

Thermal expansion expresses itself, on a microscopic scale, by a change of the interplanar spacings of lattice planes. These can be measured by use of diffraction methods from changes of Bragg angles θ. Differentiation of the Bragg equation $2d \sin\theta = \lambda$, giving $\Delta d/d = -\cot\theta\Delta\theta$, yields the thermal expansions α'_{11} in directions normal to lattice planes (hkl) (*i.e.* along $\mathbf{h} = h\mathbf{a}^* + k\mathbf{b}^* + l\mathbf{c}^*$) and, if $\mathbf{h}$ has direction cosines $a^{(hkl)}_{1j}$ with respect to the chosen Cartesian coordinate system,

$$\alpha'^{(hkl)}_{11} = a^{(hkl)}_{1i} a^{(hkl)}_{1j} \alpha_{ij} = \frac{1}{d^{(hkl)}} \frac{\partial d^{(hkl)}}{\partial T} = -\cot\theta \frac{\partial\theta}{\partial T}.$$

The coefficient $\cot\theta$ permits a tremendous increase of sensitivity and accuracy if $\theta \to 90°$. That means, if possible, high-angle $(\theta > 70°)$ reflections should be used for measurement because, for a given Δd, the changes of Bragg angles $|\Delta\theta|$ to be measured increase with $(\cot\theta)^{-1} = \tan\theta$.

The most important diffraction techniques (X-radiation is preferentially used) are: the rotating-crystal method, the Weissenberg method and diffractometers with counter recording. If small single crystals (> approximately 50 μm) are not available, powder methods (using a Debye–Scherrer film camera or powder diffractometer) must be used, although the advantage of the highly accurate back-reflections, in general, cannot be used.

Experimental aspects of measuring absolute d-values are discussed in detail in Volume C of *International Tables for Crystallography* (1999), Part 5. Since only relative displacements are to be measured in the present case, many complications connected with the determination of absolute values do not apply for thermal expansion measurements, such as zero-point correction, eccentricity of the mounted sample, refraction, absorption and diffraction profile.

1.4.3.3. *Optical methods (interferometry)*

The basic principle of measuring thermal expansion by interferometry consists of converting sample-length changes into variations of optical path differences of two coherent monochromatic light beams, which are reflected from two opposite end faces of the sample (or planes corresponding to them). An He–Ne laser usually serves as a light source. A beam expander produces a parallel beam and interference by two planes, which are slightly inclined to each other, produces fringes of equal thickness. Thermal expansion causes a movement of this fringe pattern, which is detected by photodiodes. The number of fringes passing a reference mark is counted and gives a measure of the relative movement of the two planes.

As examples for various realizations of interferometric devices (Hahn, 1998), two basic designs will be described.

(i) *Fizeau interferometer* (Fig. 1.4.3.1). The sample S is covered by a thin plate P_2 (with a polished upper surface and a coarsely ground and non-reflecting lower surface) and is placed in between a bottom plate P_3 and a wedge-shaped plate P_1 (wedge angle of about 1°). The upper surface of P_1 reflects the incident beam (i) to a reflected beam (r) so that it is removed from the interference process. The relevant interference takes place between ray (1) reflected by the lower surface of P_1 and ray (2) reflected by the upper surface of P_2. A cylindrical tube T, which defines the distance between P_1 and P_3 as well as P_2, is usually made of fused silica, a material of low and well known thermal expansion. The measured dilatation is caused, therefore, by the difference between thermal expansion of the sample and a portion of the fused silica tube of equal length. The whole apparatus is mounted in a thermostat.

(ii) *Michelson interferometer* (Fig. 1.4.3.2). The reference mirror M and the beam-splitter B are placed outside the thermostat. The upper face of the sample S is one interference plane and the upper surface of the bottom plate is the other. The

interference pattern IP is divided into two fields corresponding to the two ends of the sample. The difference of fringe movements within these two fields yields the absolute thermal expansion of the sample.

1.4.3.4. *Electrical methods*

1.4.3.4.1. *Inductance changes (pushrod dilatometry)*

With this method, the expansion of the crystal is transmitted out of the cooled or heated region to an external measuring device by a rod made of a reference material whose thermal expansion is low and well known (usually silica glass) (*cf.* Gaal, 1998). If this rod is inside a tube of the same material (silica glass), and the specimen is inside as well, then the difference in expansion between the crystal and an equal length of the reference material is measured. Above 1100 K, instead of silica glass, high-purity alumina or single-crystal sapphire or tungsten rods are used.

To measure the displacement of the rods, several techniques are used. The most important are:

(1) a ferrite core is moved in a coil to change the inductivity of the coil, which is detected by the change of resonance frequency of an electrical circuit having a fixed capacitance;

(2) linear-variable-differential transformers.

Temperature gradients in the rod and the tube can lead to severe complications. For every determination, the system should be calibrated by certified materials (White, 1998), such as α-Al_2O_3, Cu, Pt, fused silica, Si, W, Mg or Mo.

1.4.3.4.2. *Capacitance methods*

In a way similar to the interferometric methods, the change of the gap between the lower surface of P_1 and the upper surface of P_2 (Fig. 1.4.3.1) is used to determine the thermal expansion of the sample. This gap – with electrically conducting surfaces – is used as the capacitance in an electric circuit with a fixed inductance. The change of capacitance leads to a change of resonance frequency, which is measured.

1.4.4. Relation to crystal structure

The anharmonicities of the interatomic potentials gain importance with increasing vibration amplitudes of the atoms. Since, at a given temperature, weakly bonded atoms oscillate with larger amplitudes, they contribute to a larger degree to thermal expansion in comparison with stronger bonds. This correlation follows also from the Grüneisen relation (1.4.2.14) because α (or β) is proportional to the compressibility, which, in turn, is a rough measure of the interatomic and intermolecular forces.

This simple consideration allows qualitative predictions of the thermal expansion behaviour of a crystal species if the structure is known:

(1) Covalent bonds are associated with very small thermal expansions (diamond, graphite perpendicular to the *c* axis), whereas van der Waals bonds give rise to large thermal expansions (N_2, graphite parallel to the *c* axis). In accordance with their relatively high elastic stiffness, hydrogen bonds, especially short hydrogen bonds, lead to comparably small thermal expansions.

(2) In layer-like structures, the maximum thermal expansion occurs normal to the layers (mica, graphite, pentaerythritol).

(3) Thermal expansion decreases when the density of weak bonds decreases: therefore, expansion is greater for crystals with small molecules (many van der Waals contacts per volume) than for their larger homologues (*e.g.* benzene–naphthalene–anthracene).

Buda *et al.* (1990) have calculated the thermal expansion of silicon by means of *ab initio* methods. It is to be expected that these methods, which are currently arduous, will be applicable to more complicated structures in the years to come and will gain increasing importance in this field (*cf.* Lazzeri & de Gironcoli, 1998).

It is observed rather frequently in anisotropic materials that an enhanced expansion occurs along one direction and a contraction (negative expansion) in directions perpendicular to that direction (*e.g.* in calcite). The volume expansion, *i.e.* the trace of α_{ij}, is usually positive in these cases, however. If the tensor of elastic constants is known, such negative expansions can mostly be explained by a lateral Poisson contraction caused by the large expansion (Küppers, 1974).

Only a few crystals show negative volume expansion and usually only over a narrow temperature range (*e.g.* Si and fused silica below about 120 K and quartz above 846 K) (White, 1993). Cubic ZrW_2O_8 was recently found to exhibit isotropic negative thermal expansion over the complete range of stability of this material (0.5–1050 K) (Mary *et al.*, 1996). This behaviour is explained by the librational motion of practically rigid polyhedra and a shortening of Zr—O—W bonds by transverse vibration of the oxygen atom. By tailoring the chemical content (of TiO_2 or

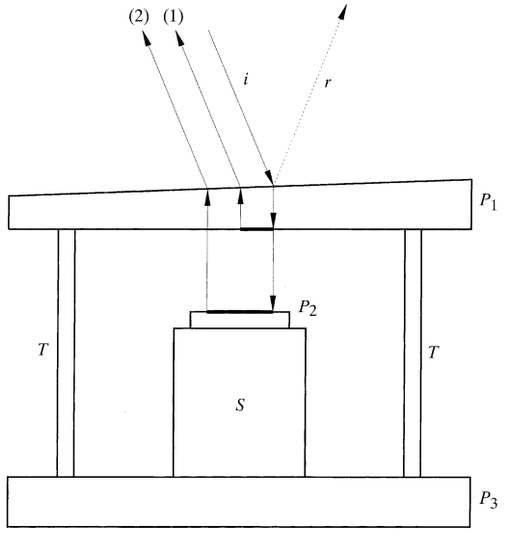

Fig. 1.4.3.1. Schematic diagram of a Fizeau interferometer.

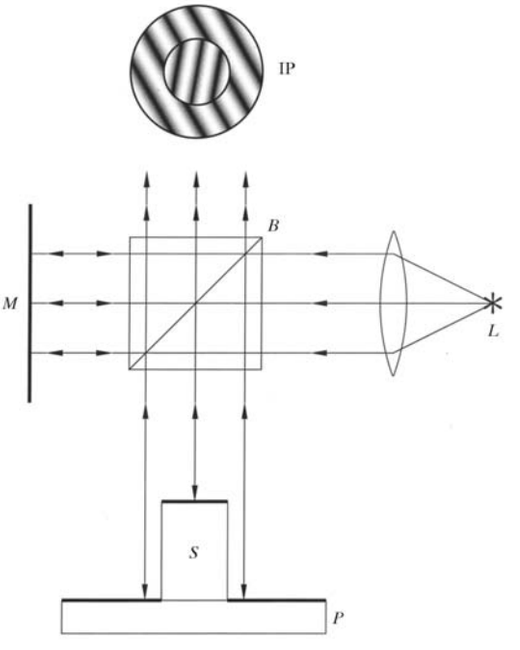

Fig. 1.4.3.2. Schematic diagram of a Michelson interferometer.

$LiAlSiO_4$) in a glassy matrix, an expansion coefficient can be achieved that is nearly zero over a desired temperature range.

A compilation of numerical values of the tensor components of more than 400 important crystals of different symmetry is given by Krishnan *et al.* (1979).

Phase transitions are accompanied and characterized by discontinuous changes of derivatives of the free energy. Since the thermal expansion β is a second-order derivative, discontinuities or changes of slope in the $\beta(T)$ curve are used to detect and to describe phase transitions (*cf.* Chapter 3.1).

1.4.5. Glossary

α_{ij}	thermal expansion
β	volume thermal expansion
γ	Grüneisen parameter
κ	isothermal compressibility
u_{ij}	strain tensor
c^V	specific heat at constant volume
F	free energy
p	pressure
S	entropy
T	temperature
V	volume

References

Barron, T. H. K. (1998). *Generalized theory of thermal expansion of solids.* In *Thermal expansion of solids*, edited by C. Y. Ho, ch. 1. Materials Park, Ohio: ASM International.

Buda, F., Car, R. & Parrinello, M. (1990). *Thermal expansion of c-Si via ab initio molecular dynamics. Phys. Rev. B*, **41**, 1680–1683.

Gaal, P. S. (1998). *Pushrod dilatometers.* In *Thermal expansion of solids*, edited by C. Y. Ho, ch. 5. Materials Park, Ohio: ASM International.

Hahn, T. A. (1998). *Thermal expansion measurements using optical interferometry.* In *Thermal expansion of solids*, edited by C. Y. Ho, ch. 6. Materials Park, Ohio: ASM International.

International Tables for Crystallography (1999). Vol. C. *Mathematical, physical and chemical tables*, 2nd ed., edited by A. J. C. Wilson & E. Prince. Dordrecht: Kluwer Academic Publishers.

Jessen, S. M. & Küppers, H. (1991). *The precision of thermal-expansion tensors of triclinic and monoclinic crystals. J. Appl. Cryst.* **24**, 239–242.

Krishnan, R. S., Srinivasan, R. & Devanarayanan, S. (1979). *Thermal expansion of solids.* Oxford: Pergamon.

Küppers, H. (1974). *Anisotropy of thermal expansion of ammonium and potassium oxalates. Z. Kristallogr.* **140**, 393–398.

Lazzeri, M. & de Gironcoli, S. (1998). *Ab initio study of Be(001) surface thermal expansion. Phys. Rev. Lett.* **81**, 2096–2099.

Mary, T. A., Evans, J. S. O., Vogt, T. & Sleight, A. W. (1996). *Negative thermal expansion from 0.3 to 1050 Kelvin in ZrW_2O_8. Science*, **272**, 90–92.

Nye, J. F. (1985). *Physical properties of crystals.* Oxford: Clarendon Press.

Saxena, S. K. & Shen, G. (1992). *Assessed data on heat capacity, thermal expansion, and compressibility of some oxides and silicates. J. Geophys. Res.* **97**, 19813–19825.

Schlenker, J. L., Gibbs, G. V. & Boisen, M. B. (1978). *Strain-tensor components expressed in terms of lattice parameters. Acta Cryst.* A**34**, 52–54.

White, G. K. (1993). *Solids: thermal expansion and contraction. Contemp. Phys.* **34**, 193–204.

White, G. K. (1998). *Thermal expansion reference materials*. In *Thermal expansion of solids*, edited by C. Y. Ho, ch. 11. Materials Park, Ohio: ASM International.